I R A M P
7(2), Dec. 2016, pp. 73-80

ISSN: 2229-3159

Dielectronic Recombination of W^{28+}

M. S. PINDZOLA[1], S. D. LOCH[1], AND J. P. COLGAN[2]

[1] Department of Physics, Auburn University, Auburn, AL
[2] Theoretical Division, Los Alamos National Laboratory, Los Alamos, NM

ABSTRACT: Dielectronic recombination Maxwellian rate coefficients for W^{28+} in its ground state are carried out using a configuration-average distorted-wave method. The accuracy of the results are established by examining the close to threshold W^{27+} recombined $4s^24p^64d^94f8d$ configuration. The configuration-average cross section at 7.65 eV above threshold is found to be quite different from the 176 statistically-partitioned level-resolved cross sections ranging from -10.6 eV below threshold to 52.9 eV above threshold. Dielectronic recombination Maxwellian rate coefficients using the configuration-average and the statistically-partitioned level-resolved methods are also found to be quite different at low temperatures. Dielectronic recombination Maxwellian rate coefficients are calculated using a configuration-average distorted-wave method for all the W^{27+} recombined $4s^24p^64d^94fnl$, $4s^24p^5\ 4d^{10}4fnl$, $4s4p^64d^{10}4fnl$, and $4s^2\ 4p^6\ 4d^9\ 5l'\ nl$ ($l' = 0 - 3$) configurations. We find large differences between the configuration-average and recent intermediate-coupled level-resolved rate coefficients at low temperatures and a factor of 2 difference at intermediate temperatures around 50 eV.

1. INTRODUCTION

Due to the importance of high-Z plasma facing components in magnetically confined fusion experiments, there has been a lot of interest in using heavy elements in current and future fusion experiments. They are able to withstand high heat loads and have low sputtering. Molybdenum is of interest as a possible plasma facing component and has been tested at Alcator C-Mod[1] and the National Spherical Torus Experiment (NSTX) Upgrade[2]. Tungsten is also of interest and has been tested at the Joint European Torus (JET)[3] and the Axially Symmetric Divertor Experiment (ASDEX) Upgrade[4]. Other possible elements include Zr, Nb, Hf, and Ta[5]. Thus, the atomic data for such heavy elements is of critical importance for fusion energy research. For low charge states, the atomic data is used in wall erosion measurements, while data for all of the charge states is important for impurity transport modeling and power loss studies from the plasma core.

Much recent work has been performed on the atomic data for tungsten. This has included work on electron-impact ionization for W^{19+} [6] and W^{27+} [7, 8], as well as dielectronic recombination for W^{18+} [9], W^{19+} [10], W^{20+} [11, 12, 13], W^{28+} [14, 15], and W^{35+} [16]. Since recent cross section and Maxwellian rate coefficient calculations for W^{28+} are in poor agreement, in this paper we examine the dielectronic recombination of W^{28+} in its $4s^24p^64d^{10}$ ground state. We first focus on the close to threshold W^{27+} recombined $4s^24p^64d^94f\ 8d$ configuration. We compare configuration-average and statistically-partitioned level-resolved cross sections to find the temperatures at which their Maxwellian rate coefficients are in good agreement. By examination of a configuration near threshold we also calculate the contributions that below threshold levels may have on the Maxwellian rate coefficients, previously studied for Mg^{8+} [17] and C^{3+} [18]. We then calculate configuration-average cross sections and Maxwellian rate coefficients for all the W^{27+} recombined $4s^24p^64d^94fnl$, $4s^24p^54d^{10}4fnl$, $4s4p^64d^{10}4fnl$, and $4s^24p^64d^95lnl$ ($l' = 0 - 3$) configurations.

The rest of this paper is organized as follows. In Section II we give a brief review of the configuration-average distorted-wave theory used to calculate dielectronic recombination cross sections. In Section III we present our cross section and Maxwellian rate coefficient results for the dielectronic recombination of W^{28+}. We conclude with a brief summary and future plans in Section IV. Unless otherwise stated, we will use atomic units.

2. THEORY

The configuration-average autoionization rate for three active subshells is given by:

$$A_{auto}(n_1 l_1 n_2 l_3 n_3 l_3) = \frac{w_2 w_3 (4l_1 + 2 - w_1)}{k_e} \times (4l_e + 2)\mathcal{S}(n_2 l_2 n_3 l_3 \rightarrow n_1 l_1 k_e l_e), \tag{1}$$

where w_1, w_2, w_3 are subshell occupation numbers, $n_1 l_1$, $n_2 l_2$, and $n_3 l_3$ are quantum numbers of the bound electrons, $k_e l_e$ are quantum numbers of the ejected continuum electrons, and $\mathcal{S}(n_2 l_2 n_3 l_3 \rightarrow n_1 l_1 k_e l_e)$ are autoionization probabilities given in terms of 3j/6j symbols and radial Slater integrals[19].

The configuration-average radiative rate for two active subshells is given by:

$$A_{rad}(n_1 l_1 n_2 l_2) = \frac{8\omega^3}{3c^3} \frac{(4l_1 + 3 - w_1) w_2}{(4l_1 + 2)(4l_2 + 2)} \times \{l >\} \mathcal{S}(n_2 l_2 \rightarrow n_1 l_1), \tag{2}$$

where ω is the transition frequency, c is the speed of light, $l >$ = max(l_1, l_2), and $\mathcal{S}(n_2 l_2 \rightarrow n_1 l_1)$ are radiative probabilities given in terms of radial dipole matrix elements[19].

The bound radial orbitals needed for the calculations of the autoionization and radiative probabilities are obtained by using a Hartree-Fock semi-relativistic (HFR) atomic structure code [20]. The continuum radial orbitals needed for the calculations of the autoionization probabilities are obtained by solving the radial Schrodinger equation.

The dielectronic recombination cross section is given by:

$$\sigma = \frac{2\pi^2}{\Delta\epsilon} \sum_{i=1}^{N} \frac{g_i}{2G_i} \frac{A_i B_i}{2|\epsilon_i|}, \tag{3}$$

where N is the total number of configuration-average or level-resolved autoionizing states. In Eq. (3), $\Delta\epsilon$ is the resonance energy width, g_i the statistical weight of the autoionizing configuration or level, G_i is the statistical weight of the target configuration or level, A_i is the autoionization rate, B_i is the radiative branching ratio, and ϵ_i is the energy of the autoionizing configuration or level.

3. RESULTS

The dominant dielectronic recombination transitions for the ground state of W^{28+} are given by:

$$4s^2 4p^6 4d^{10} + e \rightarrow 4s^2 4p^6 4d^9 4fnl \tag{4}$$

involving the strong $4d \rightarrow 4f$ excitation. The configuration average energies for the nl subshells near the W^{28+} $4s^2 4p^6 4d^{10}$ total energy of -15754.951 au are given in Table 1. The W^{27+} $4s^2 4p^6 4d^9 4f$ $8d$ configuration lies 7.65 eV above threshold.

3.1. Transitions to W^{27+} $4s^2 4p^6 4d^9 4f\ 8d$

The $4s^2 4p^6 4d^9 4f\ 8d$ configuration-average autoionization rate is found to be 4.57×10^{12} Hz obtained using Eq.(1). The $4s^2 4p^6 4d^9 4f\ 8d$ configuration-average radiative rates are given in Table 2 obtained using Eq.(2), with a total value of 3.79×10^{11} Hz. Thus the radiative branching ratio is $B = 0.0766$. Using Eq.(3) with $N = 1$ and $\Delta\epsilon = 0.20$ au, for the configuration $4s^2 4p^6 4d^9 4f 8d$ with a statistical weight of $g = 1400$ and the configuration $4d^{10}$ with a statistical weight of $G = 1$, the configuration-average cross section is 291 Mb.

Table 1
W^{27+} $4s^2\ 4p^6\ 4d^9\ 4f\ nl$ Energies

Configuration	*Energy*
$4s^2 4p^6 4d^9 4f\ 7s$	-104.97 eV
$4s^2 4p^6 4d^9 4f\ 8s$	-19.43 eV
$4s^2 4p^6 4d^9 4f\ 9s$	35.28 eV
$4s^2 4p^6 4d^9 4f\ 10s$	72.41 eV
$4s^2 4p^6 4d^9 4f\ 7p$	-86.87 eV
$4s^2 4p^6 4d^9 4f\ 8p$	-8.06 eV
$4s^2 4p^6 4d^9 4f\ 9p$	42.88 eV
$4s^2 4p^6 4d^9 4f\ 10p$	77.75 eV
$4s^2 4p^6 4d^9 4f\ 7d$	-62.10 eV
$4s^2 4p^6 4d^9 4f\ 8d$	7.65 eV
$4s^2 4p^6 4d^9 4f\ 9d$	53.48 eV
$4s^2 4p^6 4d^9 4f\ 10d$	85.23 eV
$4s^2 4p^6 4d^9 4f\ 7f$	-36.49 eV
$4s^2 4p^6 4d^9 4f\ 8f$	23.99 eV
$4s^2 4p^6 4d^9 4f\ 9f$	65.56 eV
$4s^2 4p^6 4d^9 4f\ 10f$	93.09 eV
$4s^2 4p^6 d^9 4f\ 7g$	-16.95 eV
$4s^2 4p^6 d^9 4f\ 8g$	36.52 eV
$4s^2 4p^6 d^9 4f\ 9g$	73.10 eV
$4s^2 4p^6 d^9 4f\ 10g$	99.19 eV

Table 2
W^{27+} $4s^2 4p^6 4d^9 4f\ 8d$ Radiative Rates

Final Configuration	*Rate*
$4d^{10} 8d$	7.15×10^{10} Hz
$4s^2 4p^6 4d^9 4f\ 5p$	9.29×10^{10} Hz
$4s^2 4p^6 4d^9 4f\ 6p$	3.11×10^{10} Hz
$4s^2 4p^6 4d^9 4f\ 7p$	7.70×10^{9} Hz
$4s^2 4p^6 4d^9 4f\ 8p$	1.11×10^{10} Hz
$4s^2 4p^6 4d^9 4f\ 4f$	3.79×10^{10} Hz
$4s^2 4p^6 4d^9 4f\ 5f$	3.75×10^{10} Hz
$4s^2 4p^6 4d^9 4f\ 6f$	4.07×10^{10} Hz
$4s^2 4p^6 4d^9 4f\ 7f$	4.87×10^{10} Hz

Using the HFR atomic structure code[20], the $4s^24p^64d^94f\ 8d$ configuration is found to have 176 LSJ levels ranging from –10.6 eV to + 52.9 eV with respect to the $4d^{10}$ total energy. Using Eq.(3) with $N = 176$ and $\Delta\epsilon = 0.20$ au, for the configuration $4s^24p^64d^94f8d$ with a statistical weight of $g_i = 2\ J_i + 1$, $G_i = 1$, $A_i = A$, and $B_i = B$, the statistically-partitioned level-resolved cross sections range from 0.60 Mb for the $J = 1.5$ level at -10.6 eV to 0.12 Mb for the $J = 1.5$ level at +52.9 eV.

The configuration-average and statistically-partitioned level-resolved cross sections for dielectronic recombination into the $4s^24p^64d^94f\ 8d$ configuration are presented in Figure 1. The cross sections have been Gaussian convoluted using a full width at half maximum of 1.0 eV. Within ± 1.0 eV of threshold are 30 level-resolved cross sections including the $J = 6.5$ level at -0.9357 eV with a cross section of 23.8 Mb, the $J = 2$ level at -0.0865 eV with a cross section of 110.3 Mb, and the $J = 2.5$ level at 0.793 eV with a cross section of 12.0 Mb.

Configuration-average and statistically-partitioned level-resolved Maxwellian rate coefficients are calculated for dielectronic recombination into the $4s^24p^64d^94f8d$ configuration. In Figure 2 the 55 levels that lie below the threshold are ignored. The largest differences are found below 10 eV, where at 1.0 eV the configuration-average rate is 3.1×10^{-11} cm^3 /sec and the level-resolved rate is 5.2×10^{-9} cm^3 /sec. Above 10 eV the differences are relatively small, where at 1000 eV the configuration-average rate is 2.6×10^{-12} cm^3 /sec and the level-resolved rate is 1.9×10^{-12} cm^3 /sec. In Figure 3 the 55 levels that lie below the threshold are included in keeping with the importance of near threshold states in most plasmas. The largest differences are again found below 10 eV, where at 1.0 eV the configuration-average rate is again 3.1×10^{-11} cm^3 /sec and the level-resolved rate is now 9.9×10^{-9} cm^3 /sec. Above 10 eV the configuration-average and level-resolved rates are in good agreement.

3.2. Transitions to W^{27+} $4s^24p^64d^94fnl$

Specific dielectronic recombination calculations are carried out for the $4s^24p^64d^94fnl$ configurations involving up to $n = 14$ and $l = 0 – 4$. Contributions from higher n and l are found by extrapolation along the Rydberg series. The configuration-average cross sections for dielectronic recombination into the $4s^24p^64d^94fnl$ configurations are presented in Figure 4. The cross sections have again been Gaussian convoluted using a full width at half maximum of 1.0 eV. The largest contributions are from the $4s^24p^64d^94f8l$ configurations with the $4s^24p^64d^94f8d$ configuration at 7.65 eV above threshold. The $4s^24p^64d^94f8p$ configuration lies -8.06 eV below threshold.

Configuration-average Maxwellian rate coefficients are calculated for dielectronic recombination into the $4s^24p^64d^94fnl$ configurations and presented in Figure 5. The Maxwellian rate coefficients are found to be in good agreement with AUTOSTRUCTURE[21] calculations carried out in the configuration-average mode. The peak of the Maxwellian rate coefficients is found to be around a temperature of 50 *eV* with a value of 3.6×10^{-9} cm^3/sec.

3.3. Transitions to W^{27+} $4s^24p^54d^{10}4f\ nl$, $4s4p^64d^{10}4f\ nl$, and $4s^24p^64d^9\ 5l'\ nl$ ($l' = 0 – 3$)

Specific dielectronic recombination calculations are carried out for the $4s^24p^54d^{10}4f\ nl$, $4s4p^64d^{10}4f\ nl$, and $4s^24p^64d^95l'\ nl$ ($l' = 0 – 3$) configurations involving up to $n = 12$ and $l = 0 – 4$. Contributions from higher n and l are found by extrapolation along the Rydberg series.

The largest contributions made by the $4s^24p^54d^{10}4f\ nl$ configurations are from the $4s^24p^54d^{10}4f\ 6l$ configurations with the $4s^24p^54d^{10}4f\ 6d$ configuration at 37.08 eV above threshold. The $4s^24p^54d^{10}4f\ 6p$ configuration lies -5.26 eV below threshold.

The largest contributions made by the $4s4p^64d^{10}4f\ nl$ configurations are from the $4s4p^64d^{10}4f\ 5l$ configurations with the $4s4p^64d^{10}4f\ 5f$ configuration at 75.17 eV above threshold. The $4s4p^64d^{10}4f\ 5d$ configuration lies -10.68 eV below threshold.

The largest contributions made by the $4s^24p^64d^95snl$ configurations are from the $4s^24p^64d^95s6l$ configurations with the $4s^24p^64d^95s6f$ configuration at 17.18 eV above threshold. The $4s^24p^64f^95s6d$ configuration lies -26.64 eV below threshold. The largest contributions made by the $4s^24p^64d^95pnl$ configurations are from the $4s^24p^64d^95p6l$

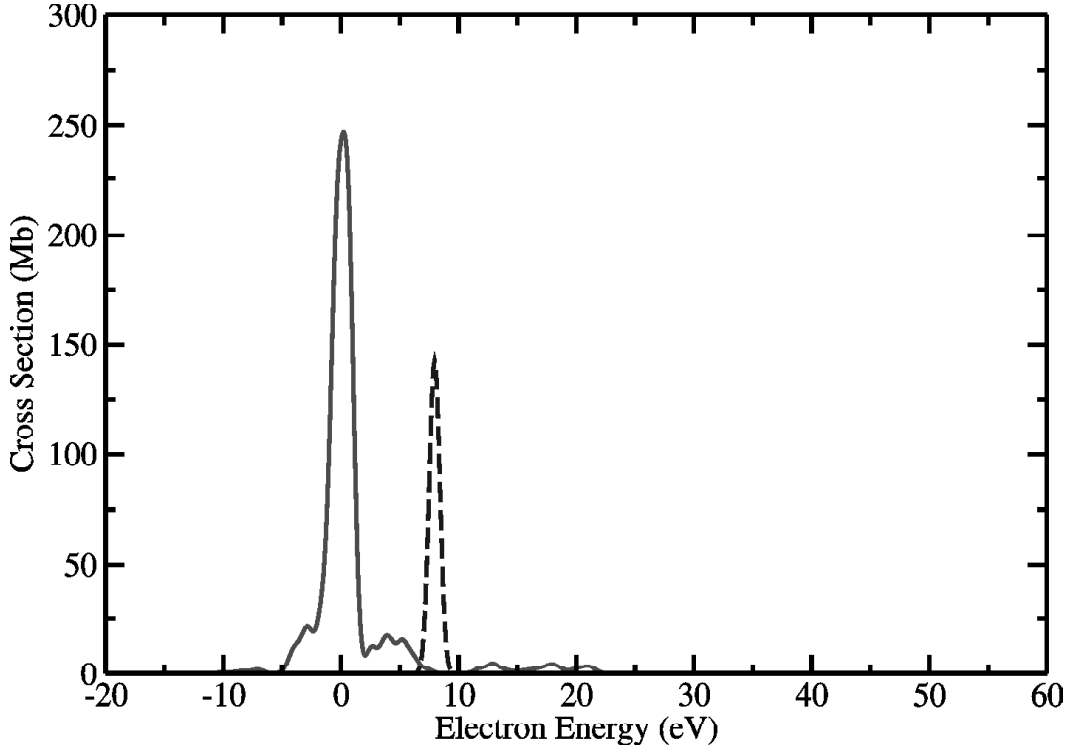

Figure 1: Dielectronic recombination cross section for $4s^2 4p^6 4d^9 4f8d$. Solid line (red): Statistically-partitioned level-resolved, Dashed line (blue): Configuration-average. (1.0 Mb = 1.0 × 10–18 cm2)

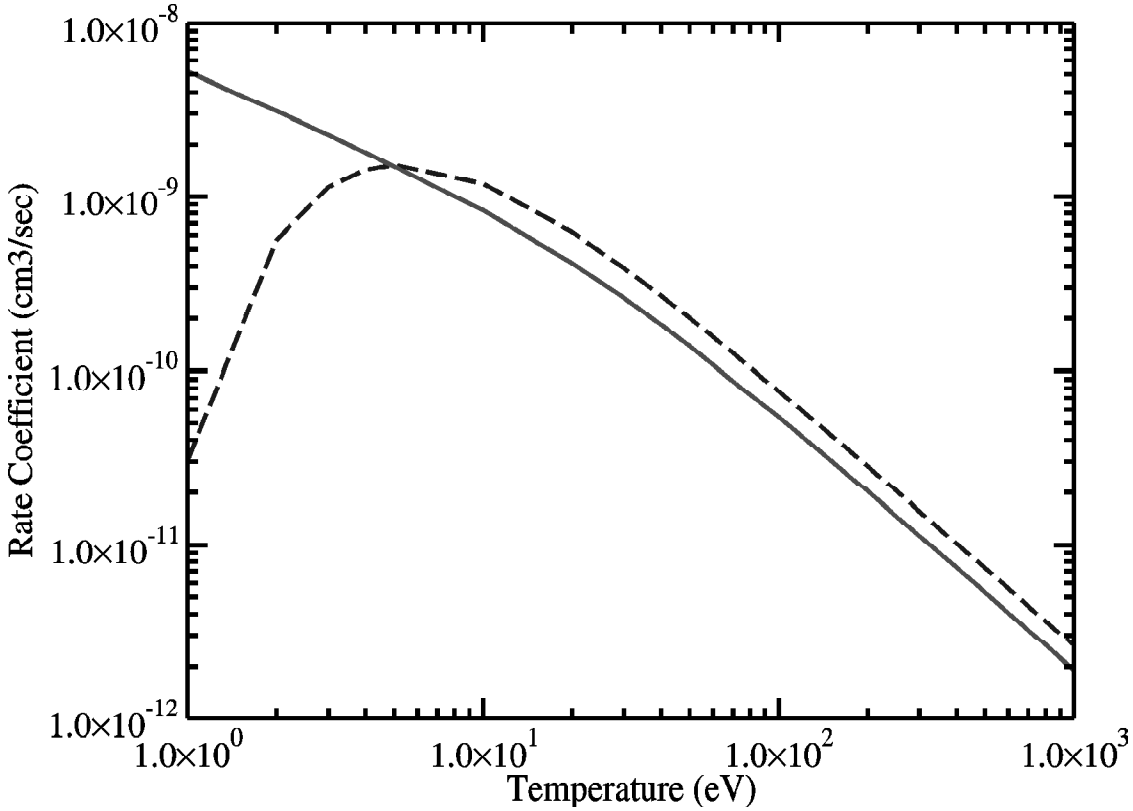

Figure 2: Dielectronic recombination Maxwellian rate coefficient for $4s^2 4p^6 4d^9 4f8d$. Solid line (red): Statistically-partitioned level-resolved for only levels above threshold, Dashed line (blue): Configuration-average

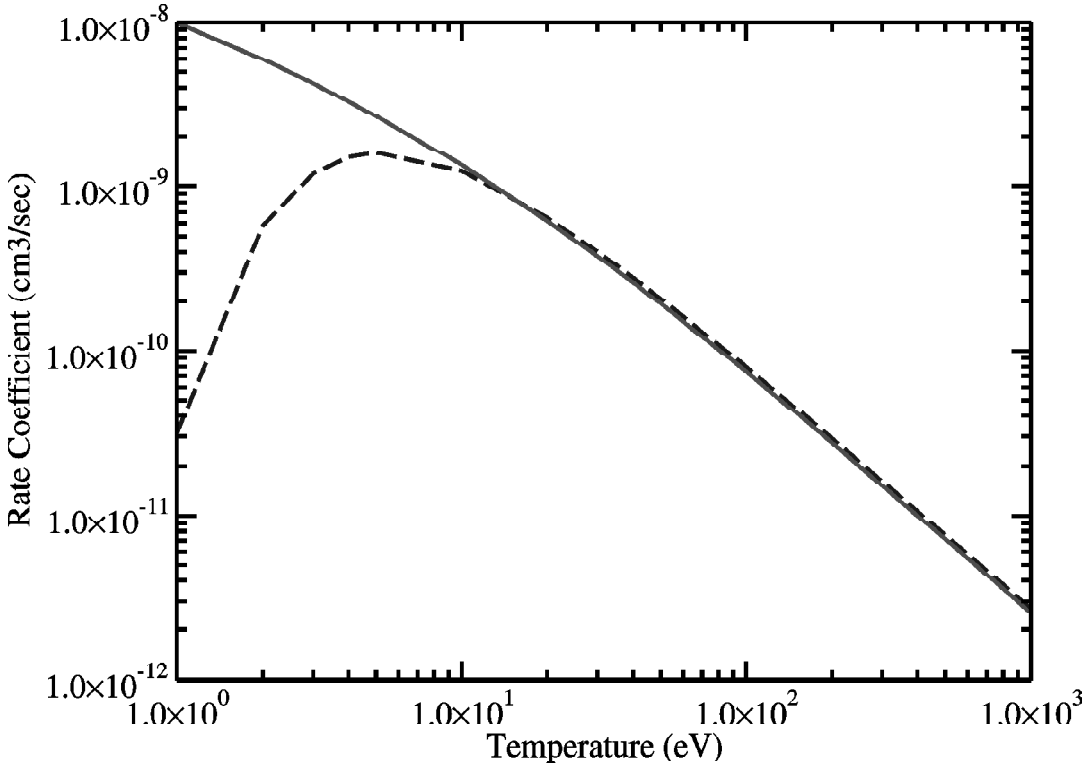

Figure 3: Dielectronic recombination Maxwellian rate coefficient for $4s^2 4p^6 4d^9 4f8d$. Solid line (red): Statistically-partitioned level-resolved for all levels above and below threshold, Dashed line (blue): Configuration-average

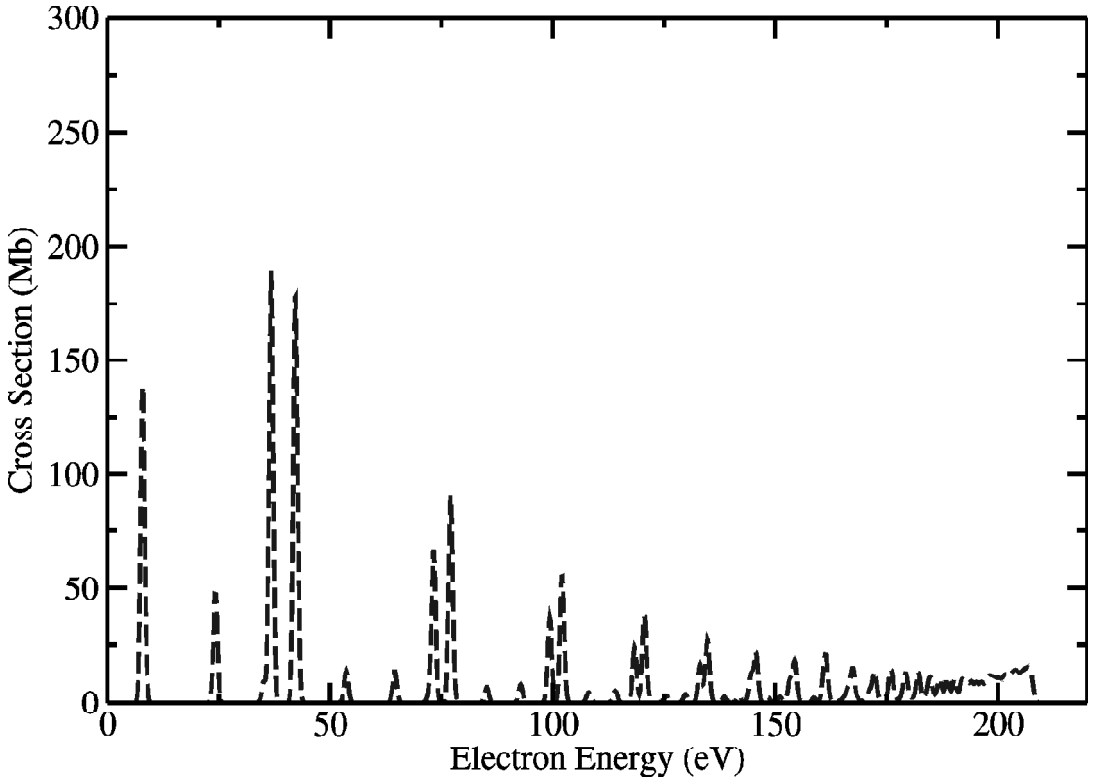

Figure 4: Dielectronic recombination cross section for $4s^2 4p^6 4d^9 4f\ nl$. Dashed line (blue): Configuration-average (1.0 Mb = 1.0×10^{-18} cm^2)

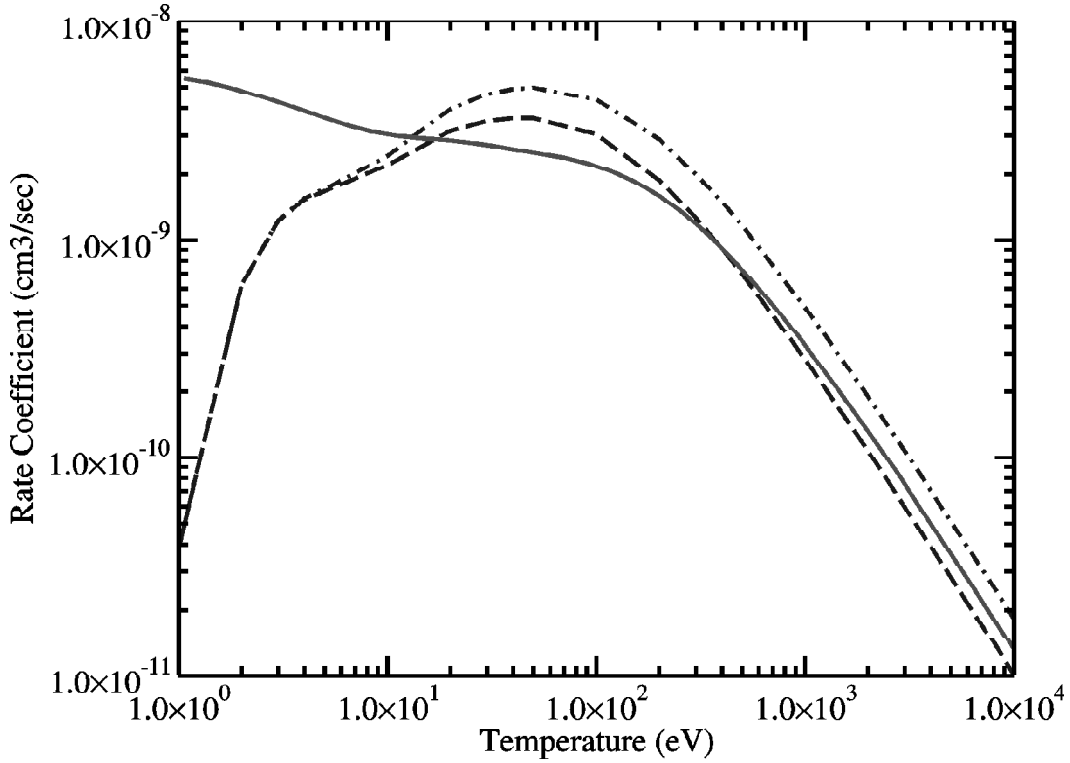

Figure 5: Dielectronic recombination Maxwellian rate coefficient. Solid line (red): Intermediate-coupled level-resolved[15], Dashed line (blue): Configuration-average for $4s^24p^64d^94f\ nl$, Dot-dashed line (blue): Configuration-average for $4s^24p^64d^94f\ nl$, $4s^24p^54d^{10}4f\ nl$, $4s4p^64d^{10}4f\ nl$, and $4s^24p^64d^95l\ nl$ (l = 0 – 3)

configurations with the $4s^24p^64d^95p6d$ configuration at 36.81 eV above threshold. The $4s^24p^64d^95p6p$ configuration lies -5.93 eV below threshold. The largest contributions made by the $4s^24p^64d^9\ 5dnl$ configurations are from the $4s^24p^64d^95d5l$ configurations with the $4s^24p^64d^95d5g$ configuration at 60.61 eV above threshold. The $4s^24p^64d^95d5f$ configuration lies -6.39 eV below threshold. The largest contributions made by the $4s^24p^64d^95f\ nl$ configurations are from the $4s^24p^64d^95f\ 5l$ configurations with the $4s^24p^64d^95f^2$ configuration at 80.31 eV above threshold.

Configuration-average Maxwellian rate coefficients are calculated for dielectronic recombination into the $4s^24p^64d^94f\ nl$, $4s^24p^54d^{10}4f\ nl$, $4s4p^64d^{10}4f\ nl$, and $4s^24p^64d^95l'\ nl$ (l = 0 – 3) configurations and presented in Figure 5. Care is taken that configurations are not double counted. The Maxwellian rate coefficients are found to be in good agreement with AUTOSTRUCTURE[21] calculations carried out in the configuration-average mode. The peak of the Maxwellian rate coefficients is found to be around a temperature of 50 eV with a value of 5.0×10^{-9} cm^3 /sec.

Maxwellian rate coefficients using an intermediate-coupled level-resolved method[15] are presented in Figure 5. At low temperatures there are large differences due to the importance of using level-resolved cross sections. At a temperature of 50 eV the intermediate-coupling results are about a factor of 2 lower than the configuration-average results. At higher temperatures the intermediate-coupling results fall between the total configuration-average results and $4s^24p^64d^94f\ nl$ configuration-average results. We note that earlier Maxwellian rate coefficients using an intermediate-coupled level-resolved method[14] are significantly lower at the higher temperatures.

4. SUMMARY

Dielectronic recombination Maxwellian rate coefficients were calculated for W^{28+} in its ground state. Calculations for the near threshold $4s^24p^64d^94f\ 8d$ configuration showed the importance of making level-resolved cross sections at temperatures below 10 eV. We also found a substantial increase in the level-resolved rate coefficient when below

threshold levels were included, the rate coefficient moving up a factor of 3 at a temperature of 1 eV.

We than calculated configuration-average cross sections and Maxwellian rate coefficients for dielectronic recombination involving $\Delta n = 0$ excitations of the 4*s*, 4*p*, and 4*d* subshells and $\Delta n = 1$ excitations of the 4*d* subshell. When compared to recent intermediate-coupled level-resolved Maxwellian rate coefficients[15], we found, as expected, large differences at low temperatures. However, at intermediate temperatures around 50 eV, the configuration-average Maxwellian rate coefficients were found to be a factor of 2 higher than recent intermediate-coupled level-resolved rates[15].

In conclusion, although the configuration-average method is computationally straightforward and can be easily used along entire isonuclear sequences for W and other heavy metals, the Maxwellian rate coefficients obtained are very poor at low temperatures and only moderately accurate at the higher temperatures.

Acknowledgments

We would like to thank Dr. Simon Preval and Professor Nigel Badnell of the University of Strathclyde for making AUTOSTRUCTURE calculations in the configuration-average mode. This work was supported in part by grants from the US Department of Energy and the US National Aeronautics and Space Administration. Computational work was carried out at the National Energy Research Scientific Computing Center (NERSC).

References

[1] Lipschultz B *et al*. 2001 Nuclear Fusion **41** 585.

[2] Kaye S M et al. 2015 Nuclear Fusion **55** 104002.

[3] Matthews G F *et al*. 2014 Physica Scripta **T159** 014015.

[4] Rohde V *et al*. 2013 Journal of Nuclear Materials **438** S800.

[5] Brooks J N, El-Guebaly L, Hassanein A, and Sizyuk T 2015 Nuclear Fusion **55** 043002.

[6] Borovik A, Ebinger B, Schury D, Schippers S, and Muller A 2016 Phys. Rev. A **93** 012708.

[7] Jonauskas V, Kyniene A, Merkelis G, Gaigalas G, Kisielius R, Kucas S, Masys S, Radziute L, and Rynkun P 2015 Phys. Rev. A **91** 012715.

[8] Pindzola M S and Loch S D 2016 Phys. Rev. A **93** 062709.

[9] Spruck K, Badnell N R, Krantz C, Novotny O, Becker A, Bernhardt D, Grieser M, Hahn M, Repnow R, Savin D W, Wolf A, Muller A, and Schippers S 2014 Phys. Rev. A **90** 032715.

[10] Badnell N R, Spruck K, Krantz C, Novotny O, Becker A, Bernhardt D, Grieser M, Hahn M, Repnow R, Savin D W, Wolf A, Muller A, and Schippers S 2016 Phys. Rev. A **93** 052703.

[11] Schippers S, Bernhardt D, Muller A, Krantz C, Grieser M, Repnow R, Wolf A, Lestinsky M, Hahn M, Novotny O, and Savin D W 2011 Phys. Rev. A **83** 012711.

[12] Badnell N R, Ballance C P, Grifin D C, and O'Mullane M 2012 Phys. Rev. A **85** 052716.

[13] Berengut J C, Harabati C, Dzuba V A, Flambaum V V, and Gribakin G F 2015 Phys. Rev. A **92** 062717.

[14] Safronova U I, Safronova A S, Beiersdorfer P, and Johnson W R 2011 J. Phys. B **44** 035005.

[15] Li B, O'Sullivan G, Dong C, and Chen X 2016 J. Phys. B **49** 155201.

[16] Ballance C P, Loch S D, Pindzola M S, and Grifin D C 2010 J. Phys. B **43** 205201.

[17] Robicheaux F, Loch S D, Pindzola M S, and Ballance C P 2010 Phys. Rev. Letts. **105** 233201.

[18] Pindzola M S, Loch S D, and Robicheaux F 2011 Phys. Rev. A **83** 042705.

[19] Grifin D C, Pindzola M S, and Bottcher C 1985 Phys. Rev. A **31** 568.

[20] Cowan R D 1981 The Theory of Atomic Structure and Spectra (Berkeley, CA: University of California Press).

[21] Badnell N R 1986 J. Phys. B **19** 3827 amdpp.phys.strath.ac.uk/autos.